Sensors & Actuators: B. Chemical 423 (2025) 136773

Contents lists available at ScienceDirect

Sensors and Actuators: B. Chemical

journal homepage: www.elsevier.com/locate/snb

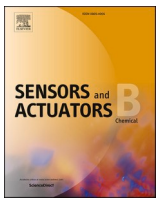

Liquid crystal gel-based acetone sensor using correlated laser speckles

Ning Bu [a,b], Yuxiang Yan [a,b], Xiaoquan Bai [a,b], Mei Wang [a,b], Yifei Ma [a,b], Suotang Jia [a,b], Xuyuan Chen [a,b], Zhaomin Tong [a,b,*]

[a] State Key Laboratory of Quantum Optics and Quantum Optics Devices, Institute of Laser Spectroscopy, Shanxi University, Taiyuan 030006, China
[b] Collaborative Innovation Center of Extreme Optics, Shanxi University, Taiyuan 030006, China

ARTICLE INFO

Keywords:
Liquid crystal gel
Laser speckle
Correlation coefficient
Acetone detection

ABSTRACT

Acetone, a common volatile organic compound (VOC), poses health risks even at low concentrations. Current acetone sensors are costly and require specialized equipment and expertize. This work develops a novel vapor sensor for determining acetone vapor concentration using the speckle patterns generated by liquid crystal gels (LCGs). The vapor sensor comprises a LCG film prepared by the phase separation of a mixture containing polystyrene microspheres and liquid crystals (LCs). The orientation of the LC molecules changes when the LCG film is exposed to an acetone vapor environment, altering the equivalent refractive indices of the LC domains. This leads to a change in the scattering state of the LCG film under laser illumination, forming different speckle patterns. The concentration of acetone vapor is determined by calculating the correlation coefficient of the speckle images, where the sensitivity and limit of detection of the sensor are 4×10^{-4} ppm^{-1} and 754.05 ppm, respectively. The developed correlated laser speckle-based optical system is simpler, less expensive, and more stable than traditional LC film vapor sensors. This acetone gas sensor has potential applications in industrial and indoor air quality testing.

1. Introduction

Rapid industrialization, urban expansion, mass transport, and intensive manufacturing activities have led to a continuous increase in emissions of volatile organic compounds (VOCs). VOCs mainly include hydrocarbons, alcohols, aldehydes, ketones, and other chemical substances that are highly volatile at room temperatures and pressures. Both natural (e.g., forests, oceans) and human (e.g., construction, fuel combustion, industrial processes) activities contribute to VOCs in the environment. VOCs pose a significant threat to human health due to their inherent toxicity and flammability. Moreover, the secondary pollutants formed by the photochemical conversion of VOCs can also negatively impact the environment. Therefore, VOC-detection technologies are essential for environmental monitoring, health management, and public safety [1,2]. Acetone is a common VOC widely used as an organic solvent in laboratory and industrial settings. It is harmful to the human nervous system and organs. Both short- and long-term exposure to high acetone concentrations pose potential health risks [3]. The Occupational Safety and Health Administration in the United States has set an 8-hour time-weighted average permissible exposure limit of 1000 ppm for acetone [4]. Concurrently, the Health and Safety Executive in the United Kingdom has specified a short-term (15 min) acetone exposure limit of 1500 ppm [5]. Exposure to acetone concentrations greater than 2000 ppm can cause dizziness, nausea, and vomiting [6]. Therefore, monitoring and preventing the leakage of high acetone concentrations into the environment is essential. Consequently, efficient, cost-effective, and accurate acetone sensors for industrial and indoor air quality detection must be developed [7].

There are various existing techniques for acetone detection. Metal oxide semiconductors-based sensors are widely used in vapor sensing [8]. However, these sensors are sensitive to humidity and typically require higher operating temperatures that may be unsafe in certain working environments. The surface plasmon resonance system can achieve real-time and reliable detection of gases [9], but this type of sensor is costly and bulky [10]. The detection methods based on surface acoustic waves and quartz crystal microbalances are sensitive to the signal-to-noise ratio and have poor selectivity [11,12]. Other methods include gas chromatography-mass spectrometry [13], proton transfer reaction mass spectrometry [14], and fluorescence quenching [15]; although these techniques provide high specificity and sensitivity, they

* Corresponding author at: State Key Laboratory of Quantum Optics and Quantum Optics Devices, Institute of Laser Spectroscopy, Shanxi University, Taiyuan 030006, China
E-mail address: zhaomin.tong@sxu.edu.cn (Z. Tong).

https://doi.org/10.1016/j.snb.2024.136773
Received 25 June 2024; Received in revised form 6 October 2024; Accepted 11 October 2024
Available online 13 October 2024

are time-consuming, labor-intensive, and require expensive laboratory equipment with trained technicians [16].

Recently, researchers have explored the use of liquid crystals (LCs) in gas-sensor technology [17–28]. LCs are stimulus-responsive materials. Certain chemical analytes can alter the orientation direction or phase properties of LCs. An LC-based miniaturized sensor can achieve real-time detection of acetone vapor at room temperature with better selectivity than the aforementioned gas-sensing methods [17]. Cholesteric LCs were reported for fabricating acetone gas sensors [18,19]. Meanwhile, nematic phase LCs were also used to detect certain VOCs [20–26]. For example, Cachelin et al. reported a novel acetone sensor based on reactive chiral dopants in nematic phase LC films [20]. The LC films were prepared by spin-coating a mixture of chiral dopants and nematic LCs onto a plane-aligned layer formed by polyimide friction coating. The reflection band of the films exposed to 1000 ppm acetone vapor for 2 h shifted by 12 nm due to the irreversible reaction between the chiral nematic LCs and acetone. Zhang et al. prepared a novel polymer-LC fiber using coaxial electrospinning technology [21]. They found that when the polymer-LC fiber was exposed to VOCs, it exhibited a rapid optical response under polarizing microscopes. Mykytyuk et al. proposed a mixture of cholesteric LC BLO-62 and nematic LC 5CB as a sensitive medium for acetone vapor optical sensors [22]. During the interaction with acetone vapor, the changed spectral characteristics of this medium was observed by a spectrophotometer. Liu et al. reported a method for measuring the two-dimensional concentration profile of toluene vapor using polymer stabilized LC [23]. After exposing the polymer stabilized LC sample to toluene vapor at 9300–2800 ppm, they analyzed the two-dimensional concentration profile using interference color changes according to different local toluene concentrations. Kooijman et al. reported an acetone sensor by utilizing the electric resistance change of LC core polymer fiber mats [24]. The LC core polymer fiber mats were fabricated by electrospinning LC-polymer solutions on substrates with interdigitated electrodes.

Most of the above-mentioned LC sensors require complex processes in the preparation of the gas-sensitive materials, some of the sensors also require expensive and complex optical analysis instruments such as polarizing microscopes, spectrophotometers, or spectrometers. Notably, due to the strong fluidity of LCs, the reported pure LC film-based sensors are limited by their poor mechanical stability and sensitivity to gravity and mechanical shock [20,25,26]. The mechanical stability of LCs can be improved by confining them within a polymer network and forming LC gels (LCGs) [27]. LCG can be prepared using a mixture of polystyrene (PS) microspheres and nematic LCs [28]. Previous studies have reported formation mechanisms of LCG that involve nucleation and growth of nematic domains followed by the expulsion of colloids during the cooling of dispersions, entanglement of topological (line) defects generated by colloidal particles in the LCs, and decomposition of helicoidal bands in the mesomorphic isotropic phase containing colloidal particle dispersions [29]. LCGs contain micron-sized LC domains that remain responsive to chemical analytes. These gels are simple to prepare and mechanically stable. The mechanical stability of LCGs enables their easy molding and processing [30].

This study develops a novel sensor for acetone vapor detection. This sensor consisted of a gas-sensitive LCG film supported on a glass substrate. The LCG film was placed in a custom-made small gas chamber and irradiated using a laser beam directed through an optical window plate installed in the chamber. This resulted in light scattering and speckle formation. A camera was positioned above the small gas chamber for real-time capturing of speckles. The response characteristics of the sensor were studied under various experimental conditions. Based on the findings, a relationship between the correlation coefficient of the speckle images and the concentration of acetone vapor was established. Finally, response time, recovery time, sensitivity, limit of detection (LOD), limit of quantification (LOQ), selectivity, consistency, repeatability, and long-term stability of the sensor were investigated. The proposed system for acetone sensing is simple, cost-effective, stable, and versatile, rendering it suitable for acetone detection in a range of fields, including industrial and indoor air quality detection.

2. Experimental part

2.1. Materials and chemicals

Styrene was purchased from Macklin Biochemical Reagent Co., Ltd. (Shanghai, China). It was washed with a 10 wt% aqueous sodium hydroxide solution to remove the inhibitor and dried with anhydrous magnesium sulfate.

Acetone, sodium hydroxide, and potassium peroxysulfate were purchased from Sinopharm Chemical Reagent Co., Ltd. (Shanghai, China). Anhydrous magnesium sulfate, anhydrous ethanol, n-hexadecane, and sodium chloride were purchased from Aladdin Biochemical Technology Co., Ltd. (Shanghai, China). Octadecyl trichlorosilane was purchased from Macklin Biochemical Reagent Co., Ltd. (Shanghai, China). Decon-90 was purchased from Decon Company (UK), and 5CB LCs were purchased from Xianhua Technology Group Co., Ltd. (Yantai, China). All chemicals were used as received.

2.2. Preparation of PS particles

PS particles were synthesized via an improved soap-free emulsion polymerization method [31,32], where a four-neck flask, reflux condenser, constant-pressure funnel, mechanical stirrer, constant-temperature water bath, and nitrogen gas inlet were used for synthesizing. 10 g of styrene, 100 g of deionized water, and sodium chloride (with varying masses of 0 g, 0.1 g, 0.2 g, and 0.3 g to obtain PS particles of different sizes) were added to the four-neck flask at room temperature. Nitrogen gas was introduced to purge oxygen from the reaction apparatus. The reaction mixture was stirred continuously for 15 min to ensure uniform dispersion of styrene in the aqueous solution. The target temperature of the water bath was then set to 70 °C, and the stirrer speed was adjusted to 250 rpm. Potassium persulfate (0.1 g) dissolved in deionized water (20 g) was used as the initiator solution. Upon reaching the set temperature, the initiator solution was rapidly added to the reaction flask to initiate polymerization. The reaction was continued in a nitrogen atmosphere for 24 h, after which the emulsion was cooled to room temperature to stop polymerization. The formed particles were repeatedly centrifuged and redispersed in deionized water to remove the unconverted styrene in the emulsion. Finally, the particles were dispersed and stored in an ethanol/water solution. As shown in Fig. S1 and Fig. S2, an increase in the mass of the sodium chloride led to an increase in ionic strength. This resulted in a thinner latex particle double layer and decreased electrostatic repulsive force between the particles initially formed. Consequently, the stability of the reaction system decreased, and the particles aggregated, forming larger PS particles [31,33]. It is worth mentioning that 0.52 μm was the smallest particle size we could achieve by the improved soap-free emulsion polymerization method, where sodium chloride was not added to the solutions.

2.3. Cleaning of glass slides and silanization of cover slides

All glass slides were treated for 15 min in a 5 % (v/w) Decon-90 solution at 40 °C and then ultrasonicated to remove surface contaminants. Subsequently, they were thoroughly rinsed with deionized water to remove remaining contaminants and cleaning agent residues. After rinsing, the slides were dried with nitrogen gas. The cover slides were placed in a Petri dish containing 0.2 mL of octadecyltrichlorosilane diluted with 20 mL of n-hexadecane. The Petri dish was covered with a sealable film and allowed to stand for 15 min. In the next step, the cover slides were sequentially placed in pure n-hexadecane, acetone, and anhydrous ethanol baths for 5 min each and finally dried in an oven at 50 °C.

2.4. Preparation of LCG film

The LCG films were prepared by slightly modifying the method reported in existing literature [28]. A schematic of the LCG film preparation process is shown in Fig. 1. 5CB LCs with a nematic-to-isotropic phase transition temperature of ~35 ℃ were used to prepare gas-sensitive materials. PS particles were washed three times by centrifugation for 10 min at 9000 rpm followed by resuspension in deionized water. The washed particles were ultrasonically dispersed in deionized water and allowed to dry at room temperature (22 °C) for three days. 5CB LCs were mixed with the dried PS particles in a desired mass ratio. The mixture was again ultrasonicated for 6 h at 60 °C to ensure uniform dispersion of the PS particles. The mixed solution was then cooled to 22 °C at a fixed rate (0.2 °C/min) in an oven to form an LCG block. A small amount of the LCG formed was placed on a clean glass slide (processed by sandblasting to enhance scattering) and heated on a hot stage to a temperature above the nematic-to-isotropic phase transition temperature of 5CB. A 5 μm thick polyethylene terephthalate (PET) film was placed around the LCG on the glass slide as a spacer, which determined the thickness of the obtained LCG films. When the composite material became transparent, a preheated (60 °C) and hydrophobically treated cover slide was placed on top of the LCG on the base glass slide. The base and top slides were clamped together with long tail clips. The components were initially cooled to 37 °C at a fixed rate (0.2 °C/min), and then they were annealed with different time periods (0–60 h). Subsequently, the film was further cooled to room temperature (22 °C) at a rate of 0.2 °C/min. Finally, the top cover slide was removed.

2.5. Material characterization

Ion sputtering (MC1000, Hitachi, Japan) was used to gold-coat the PS microspheres deposited on the glass substrates to mitigate the charging effects on the sample. A field-emission scanning electron microscope (SU8010, Hitachi, Japan) was used to characterize the morphology of the PS particles at an acceleration voltage of 5 kV. A transmission reflection polarizing microscope (59XC-PC, Shanghai Optical Instrument, China) was used to study the morphology of the nematic LC domains within the LCG films.

2.6. Detection system and sensor exposure to analyte vapors

The details of the vapor detection system are shown in Fig. 2. The analyte vapor generated by the bubbler system was fed to the cage-type optical system. The bubbler system mainly consists of gas sources, polytetrafluoroethylene guide tubes, three mass flow controllers (MFCs), pressure gauge, bubbler, thermostatic water bath, and gas mixing chamber. Dry nitrogen as a carrier gas entered into the bottom of a bubbler containing liquid organic solvent to drive the analyte vapor upward [34,35]. The bubbler was placed in a constant-temperature water bath. The saturation of the analyte vapors could be proved by the pressure gauge, where the pressure increased from the atmospheric pressure of 92 kPa to a constant value of 95 kPa after about 3 h bubbling. The analyte vapor was diluted to the desired concentration by mixing nitrogen in the gas mixing chamber. The flow of carrier gas was controlled by MFC1 (Alicat, USA) and the flow of dilution gas was controlled by MFC2 and MFC3 (Seven Star, China). In our experiment, different concentrations of analyte vapors were obtained by varying both the carrier gas flow rate to 5–50 sccm and the dilution gas flow rate to 0–2000 sccm (the flow rates of MFC2 and MFC3 are 0–1000 sccm). The lowest acetone concentration of about 600 ppm can be obtained by the bubbler system (S2 in Supplementary Information) [34–36]. A VOC detector (Skyeaglee, China) based on the principle of photoionization detection quantified the obtained concentration of analyte. The quantified analyte concentration values were consistent with the desired values. The analyte vapor was conveyed into a small, customized gas chamber containing the sensor through a polytetrafluoroethylene guide tube. The chamber body consisted of inlet and outlet holes. The optical components used in the experiments were integrated into a cage-style optical system. The bottom and top of the chamber were equipped with transparent optical window plates. The beam emitted by the laser (PL201, Thorlabs) passed through the window at the bottom of the gas chamber and illuminated the LCG film, generating speckles. A camera (CS165MU/M, Thorlabs) was placed directly above the gas chamber to capture the speckle images.

2.7. Vapor detection principle using correlated laser speckles

Fig. 3(a) shows the gas-sensing mechanism of the LCG film. The film contained confined micron-sized LC droplets within a polymer network formed by the phase separation of the PS microspheres and LC mixture. The PS colloids induced a tangential anchoring force on 5CB LCs in the nematic phase [37]. In LC molecules, the primary intermolecular forces are dipole-dipole interactions along with intermolecular van der Waals forces. Due to the existence of these forces, the long axes of the LC molecules had an orderly orientation, keeping the LCs in a stable nematic phase. Vapor diffusion of VOCs in LCs interfered with the interaction between LC molecules, destroyed the long-range order of LC molecules, and further caused the LCs to change from nematic phase to isotropic phase [38]. When the VOC vapor was removed, due to the presence of concentration gradient, the VOC gas molecules dissolved in the LCs underwent reverse diffusion, detached from the LCs, and restored them to the nematic phase.

The refractive index of PS microspheres is constant, and the different refractive indices of LCs and polymer matrix resulted in light scattering when the LCG film was laser irradiated. The scattered light interfered with the surrounding space, creating randomly distributed patterns of light and dark spots, referred to as speckles [39]. When the LCG film was exposed to VOCs, the equivalent refractive index of the LC domain changed due to the rearrangement of LC molecules, which ultimately led to the change in the speckle pattern. The correlation coefficient was used to describe the correlation between the two speckle patterns [40]. The correlation coefficient $\rho_{i,j}$ between any two speckle images was calculated using Eq. (1):

$$\rho_{i,j} = \frac{Cov(I_i, I_j)}{\sigma_i, \sigma_j} \tag{1}$$

where I_i and I_j are the light intensities of the ith and jth speckle images, respectively. cov(I_i, I_j) is the covariance between I_i and I_j. σ_i and σ_j represent the standard deviations of light intensities for the ith and jth speckle image, respectively. Each speckle image was expressed as a

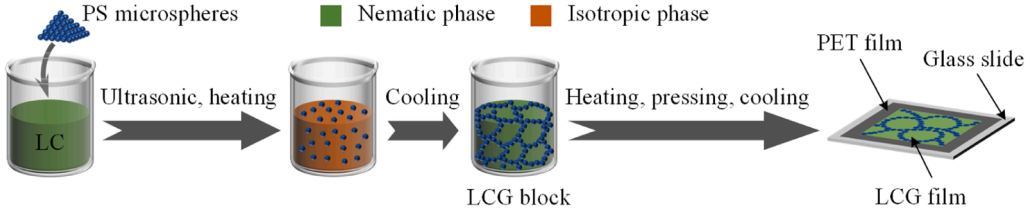

Fig. 1. Flow chart depicting the LCG film preparation method.

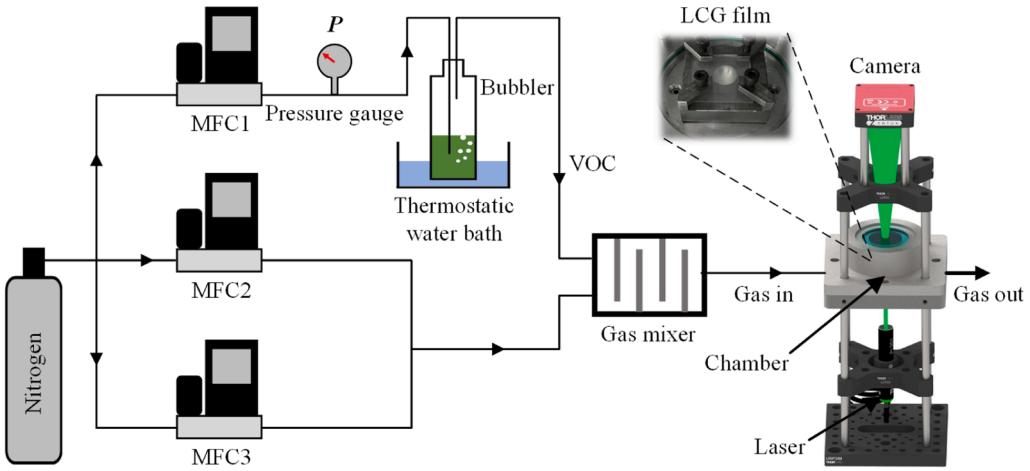

Fig. 2. Schematic of vapor detection system used in present work.

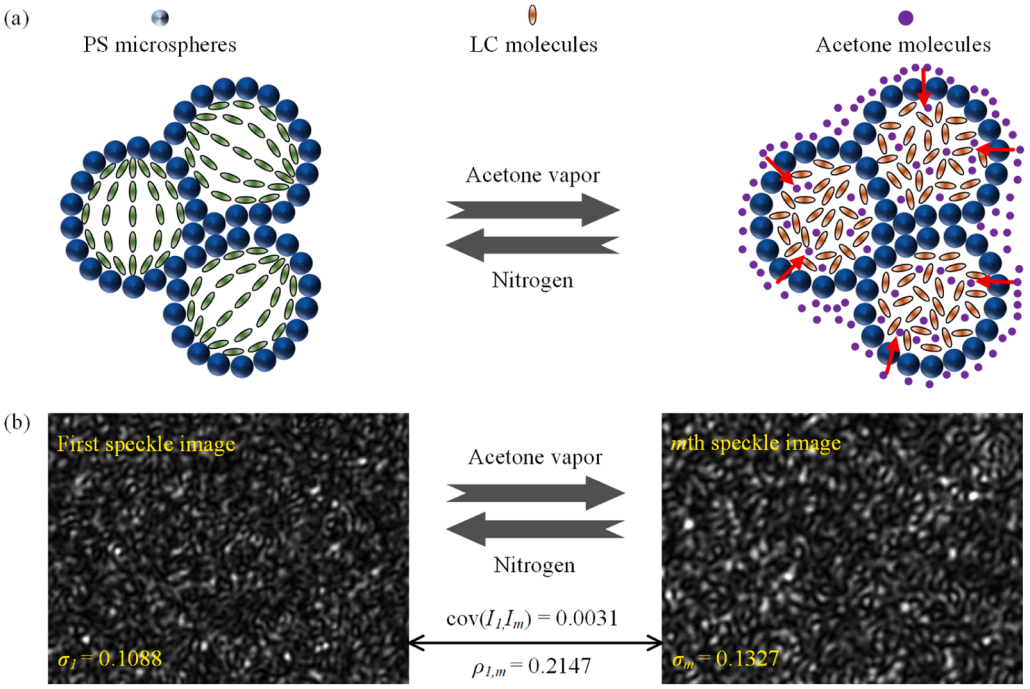

Fig. 3. (a) Schematic diagram illustrating the orientation transition of LCs and (b) speckle images in the presence and absence of acetone vapor.

matrix in Matlab. The matrix elements represented the light intensity values of the corresponding pixel points in the speckle image. Each matrix was converted into a long-column vector to calculate the covariance and standard deviation. For example, in Fig. 3(b), the first speckle image was captured before exposure to acetone vapor, and the *m*th speckle image was captured after exposure to acetone vapor with camera exposure intervals of *m*. The standard deviations of the first and *m*th speckle images were calculated with the values of $\sigma_1 = 0.1088$ and $\sigma_m = 0.1327$, respectively, and the covariance between them was $\mathrm{cov}(I_1, I_m) = 0.0031$. Therefore, the correlation coefficient between the first and *m*th speckle images was calculated as $\rho_{1,m} = 0.2147$. Similarly, the correlation coefficients between the first speckle image and other subsequent speckle images were computed sequentially such that $i = 1$ and $j = 1, 2, \ldots m\text{-}1, m\text{+}1 \ldots, N$ (where N represents the total number of speckle images captured).

3. Results and discussion

The LCG developed in this study is a composite of polymer particles and low-molecular-weight LCs. The size of the LC-rich domains affects the elastic deformation energy of the LC [41,42]. Previous studies have shown that the size of the LC-rich domains can be regulated by altering the mass fraction of PS microspheres in the LCG or the annealing time of the mixture near the LC phase transition temperature [27,43]. Hence, the microscopic morphologies of the LCG films and their responses to acetone vapor were investigated under different experimental conditions. Each film was placed in a small gas chamber within a gas sensor system to investigate its response to acetone vapor. Subsequent speckle images were captured at 5 s intervals by a camera. During the initial 300 s, pure dry nitrogen gas was delivered into the gas chamber through an inlet port. Subsequently, bubble-generated acetone vapor of concentration 1800 ppm was introduced into the chamber for 900 s. Finally, pure dry nitrogen gas was used to purge the acetone vapor inside the chamber. The gases inside the chamber were exhausted through an

outlet port and eventually released into an environment via ventilation equipment. It has been documented that VOCs reduces the nematic-isotropic phase transition temperature of LC, which leads to the orientation transition of LC molecules [44]. This indicates that the response sensitivity of acetone gas sensor increases as the ambient temperature rises, thus all tests were conducted at a constant room temperature (22 °C).

3.1. Influence of annealing time on the size of the LC-rich domains and film response

In the experiment, we observed that most of the LC-rich domains in the LCG exhibited bipolar anchoring configurations, characterized by the presence of "boojum" defects at the two opposite poles of the droplets (refer to Fig. S3 in Supplementary Information). This may be influenced by the tangential anchoring of LC molecules on the particle surface and the size of the LC droplet [45]. Figs. S4(a)-(h) in Supplementary Information show the average size of LC-rich domains (6.45 μm, 7.43 μm, 8.92 μm and 11.09 μm, respectively) obtained at different annealing times (0 h, 6 h, 12 h and 24 h) using PS microspheres with a particle size and mass fraction of 1.22 μm and 15 wt%, respectively. The size of the LC-rich domains increased with increasing annealing time of the mixture near the LC phase-transition temperature. This can be attributed to the fact that the annealing time affects the diffusive ripening of the microstructure after phase separation [43]. When the annealing time increases, LC domains have sufficient time to diffuse and their size increases accordingly. However, the diffusion slows down and gradually stops after a period of time. Fig. S5 in Supplementary Information shows that the size of the LC-rich domains remains almost unchanged under longer annealing times (36 h, 48 h, and 60 h).

Fig. S6 presents the response of the LCG film to acetone vapors observed at different annealing times using a fixed PS microsphere particle size and mass fraction of 1.22 μm and 15 wt%, respectively. The correlation coefficient of the speckle images remained close to one in a nitrogen environment, indicating that the LCG film did not respond to the nitrogen gas. However, when the film was exposed to acetone vapor, the correlation coefficient gradually decreased and eventually stabilized with time. This suggested that the absorption of acetone vapor by the LC domains in the film increased with time before reaching saturation, which induced a corresponding change in the arrangement of the LC molecules. Subsequently, the acetone vapor in the chamber was removed by blowing nitrogen (~900 s). This led to a steady increase in the correlation coefficient again to a value close to one. Eventually, the acetone in the LC domains was completely removed, and the arrangement of the LC molecules returned to their initial state.

Fig. S6 indicates that the response of the LCG film to acetone vapor gradually increased as the annealing time during the cooling process increased. This is because the annealing time significantly affected the size of the LC-rich domains. A decrease in droplet size increased the elastic deformation energy of the LC and enhanced the intermolecular forces. Thus, a greater driving force was required to alter the arrangement of LC molecules confined within the domains, which contributed to the improved stability of the LC phase [41,42]. From Fig. S6, we can also observe that as the annealing time increases from 24 h to 48 h, the responses of the LCG film are almost identical. This is because the sizes of the LC-rich domains annealed at 24 h and 48 h are 11.09 μm and 11.02 μm, respectively. Therefore, the longest annealing times were chosen as 24 h in the following experiments.

3.2. Influence of mass fraction of PS particles on the size of the LC-rich domains and film response

Figs. S7(a)-(h) in Supplementary Information show the influence of mass fractions of PS particles (20 wt%, 15 wt%, 10 wt%, and 5 wt%) on the average size of LC-rich domains (6.63 μm, 7.43 μm, 8.21 μm and 9.3 μm, respectively) observed for PS particles of size 1.22 μm and annealing time of 6 h. The size of the LC-rich domains decreased with increasing PS microsphere mass fraction. This can be attributed to the formation of PS particles aggregates when PS particles were mixed with LCs during the exclusion process. These aggregates act as impurities at the boundaries of multiple domains. During the cooling of the mixture, an increase in the microsphere mass fraction inhibited the growth of the LC microdomain structures [46]. However, when mass fractions of PS particles are lower than 5 wt%, PS microspheres/5CB composites remain in the sol state (refer to the Fig. S8 in the supplementary file for microscopic morphology of composite material) and exhibit high fluidity [46,47].

Fig. S9 shows the response of the LCG film to acetone vapors at different PS microsphere mass fractions (5, 10, 15, and 20 wt%) at a fixed PS microsphere particle size and annealing time of 1.22 μm and 6 h, respectively. Evidently, a decrease in the mass fraction of doped PS microspheres in the LCG film increased the response of the film to acetone vapor. This can also be attributed to the influence of the size of the aforementioned LC-rich domains [41,42].

3.3. Influence of PS microsphere particle size on the size of the LC-rich domains and film response

We investigated the influence of the PS microsphere particle size on the microstructural morphology of the LCG film. Figs. S10(a)-(h) in Supplementary Information show the average size of the LC-rich domains (6.98 μm, 7.43 μm, 8.09 μm, and 8.54 μm) for different sizes of PS particles (1.7 μm, 1.22 μm, 0.74 μm, and 0.52 μm, respectively) at a fixed PS particle mass fraction of 15 wt% and annealing time of 6 h. The size of the LC-rich domains decreased with increasing PS microsphere particle size. This may be due to the fact that larger PS microspheres result in thicker "walls" of the structural domains.

Fig. S11 shows the response of the LCG film to acetone vapor with different PS microsphere particle sizes at an annealing time of 6 h and PS microsphere mass fraction of 15 wt%. A decrease in the size of PS particles increased the response of the film to acetone vapor, which may be attributed to two aspects. First, the decrease in the size of the PS particles led to an increase in the size of the LC-rich domains. Second, the nematic LCs in the area immediately adjacent to the added PS particles are generally compelled to adjust their orientation away from that determined by the far-field director, ensuring that the anchoring condition at the particle interface is met. The anchoring energy WR^2 (where W is the coupling constant) of the LC at the particle surface depends on the radius of the particle R [48,49]. Hence, a decrease in the radius of the particles can lead to relatively weaker surface anchoring.

3.4. Response of vapor sensor to different concentrations of acetone vapor

In order to obtain the best response from the LCG film, we mixed LCs with PS microspheres of particle size and mass fraction of 0.52 μm and 5 wt%, respectively. While cooling, the mixture was annealed for 24 h at a constant temperature. Fig. S12 in Supplementary Information shows that the average size of LC-rich domains contained in the LCG film obtained under optimized experimental conditions is 12.38 μm. The samples were exposed to different concentrations of acetone vapor. The results are shown in Fig. 4(a). At the saturation point of vapor absorption, the correlation coefficient of the speckle images decreased as the concentration of acetone vapor increased from 600 to 2600 ppm. In other words, the response of the LCG film to acetone vapor became more intense with increasing vapor concentration. This can be attributed to greater disturbances in the initial arrangement of the LC with an increase in the acetone vapor concentration, causing the molecules to become more disordered. It can also be observed in Fig. 4(a) that when the acetone vapor concentration is below 800 ppm, there is a marginal change in the correlation coefficient of the speckle images. As the concentration of the acetone vapor increased, the response time of the

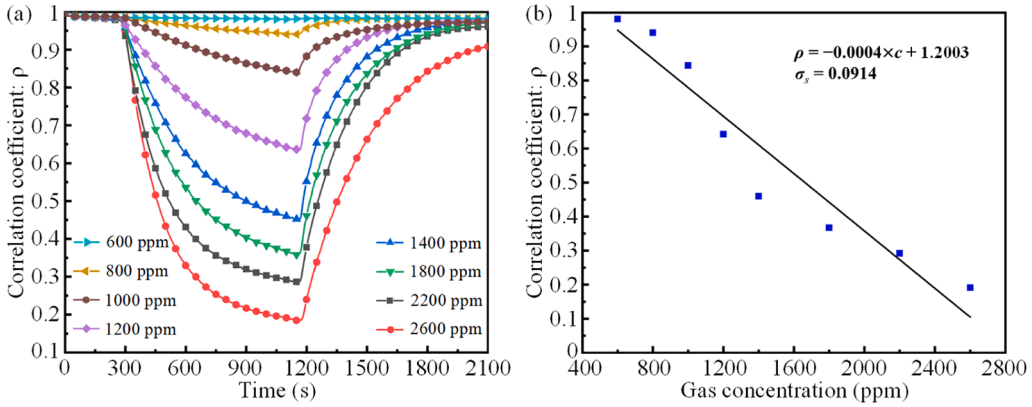

Fig. 4. (a) Response of LCG film to acetone vapor of different concentrations. (b) The correspondence between acetone gas concentration and correlation coefficient.

sensor gradually decreased, whereas the recovery time increased. This is because high concentrations of acetone vapor disrupt the order of LC molecules more easily, yet require more time to desorb from the LC-rich domains. Predictably, at an acetone vapor concentration exceeding 2600 ppm, the intermolecular forces of the acetone molecules are severely disrupted. At this point, the sensor response is no longer completely reversible. As shown in the Fig. 4(b), we extracted the speckle correlation coefficients at 1100 s and established a relationship between the concentration of acetone gas and the correlation coefficient. As the concentration of acetone gas increases, the correlation coefficient tends to decrease Therefore, it is feasible to detect acetone vapor quantitatively using the correlation coefficients of the speckle images.

3.5. Sensor performance

Response time τ_{res} is defined as the time for the variation in correlation coefficient to reach 90 % of the maximum response when exposed to acetone vapor. Whereas recovery time τ_{rec} is defined as the time needed to return to 10 % of the maximum response when exposed to nitrogen [50]. As shown in Fig. 4(a), the response time and recovery time of the sensor are $\tau_{res} = 475$ s and $\tau_{rec} = 500$ s, respectively, when exposed to 2200 ppm acetone vapor.

The sensitivity S of the sensor is defined as [51]:

$$S = \Delta\rho / c \tag{2}$$

where $\Delta\rho$ and c represent the change of correlation coefficients and acetone concentration, respectively. The sensitivity of the sensor is $S = 4 \times 10^{-4}$ ppm^{-1} according to the calculation of Fig. 4(b). The lowest amounts of gas that can be detected and accurately quantified by the sensor are LOD and LOQ, respectively. The LOD and LOQ can be calculated as [51]:

$$\mathrm{LOD} = \frac{3.3 \times \sigma_s}{S} \tag{3}$$

$$\mathrm{LOQ} = \frac{10 \times \sigma_s}{S} \tag{4}$$

where σ_s is the standard deviation, and S is the sensitivity determined by Eq. (2). After calculation of Fig. 4(b), we found $\sigma_s = 0.0914$, LOD = 754.05 ppm, and LOQ = 2285 ppm.

The key parameters of the sensor are listed in Table 1

Table 1
Sensor parameters of acetone gas sensor.

Vapor	τ_{res} (s)	τ_{rec} (s)	S (ppm^{-1})	LOD (ppm)	LOQ (ppm)
Acetone	475	500	4×10^{-4}	754.05	2285

To study the selectivity of the sensor, we exposed the sensor prepared under the optimal experimental conditions to a fixed (2200 ppm) vapor concentration of acetone, toluene, hexane, and water vapor. Based on the changes in the correlation coefficient of the speckle image shown in Fig. 5(a) (from the initial value of one to 0.279, 0.29, 0.838, 0.878, and 0.987 when exposed to acetone by air and nitrogen as the carrier gases, toluene, hexane, and water, respectively), we determined the response of the sensor to different analyte vapors as follows: acetone > toluene > hexane > water vapor. The Hansen solubility parameter δ can be used to explain the selectivity of the sensor for acetone gas [52–54]. Materials with Hansen solubility parameters that are closer to each other have higher affinity for each other and are more prone to miscibility. The Hansen solubility parameter δ can be calculated by:

$$\delta = \sqrt{\delta_D^2 + \delta_P^2 + \delta_H^2} \tag{5}$$

where δ_D, δ_P, and δ_H are London dispersion parameter, polar parameter, and electron transfer parameter, respectively. The δ_D, δ_P, and δ_H of different chemical substances in this study are listed in Table 2 [52–54], and the calculated Hansen solubility parameters δ are given in Table 2. For all test gases, the miscibility of acetone with the LC 5CB is the best, where the difference of the Hansen solubility parameters between them is the lowest.

As shown in Fig. 5(a), we also verified that acetone vapor with nitrogen or air as carrier gas elicits the same degree of response form the sensor. In addition, we exposed the three sensors prepared under the optimal experimental conditions to an acetone vapor concentration of 1400 ppm. Fig. 5(b) shows that the vapor sensor has good measurement consistency, where three LCG films were fabricated and used. Finally, we tested the long-term stability and repeatability of the sensor exposed to 2200 ppm acetone vapor during 72 h. Fig. 5(c) shows that the sensor exhibits good repeatability during long-term cyclic testing by exposing it to acetone vapor and nitrogen repeatedly.

4. Conclusion

We developed a new method for detecting acetone vapor that combines an LCG film with speckle image correlation. This method eliminates the need for complex and expensive spectral instruments and equipment, which makes it more cost-effective compared to traditional methods. The preparation of LCG films is simple and does not require complex microfabrication processes. LCG films are easy to mold and possess mechanical stability. We developed a vapor sensor that is capable of providing optimal responses for selectively detecting acetone vapor concentrations exceeding 754.05 ppm, by optimizing the annealing time during the cooling process, the mass fraction of the doped PS microspheres, and the size of the PS particles. The LCG sensor that we developed and characterized uses 5CB LC, a material with a

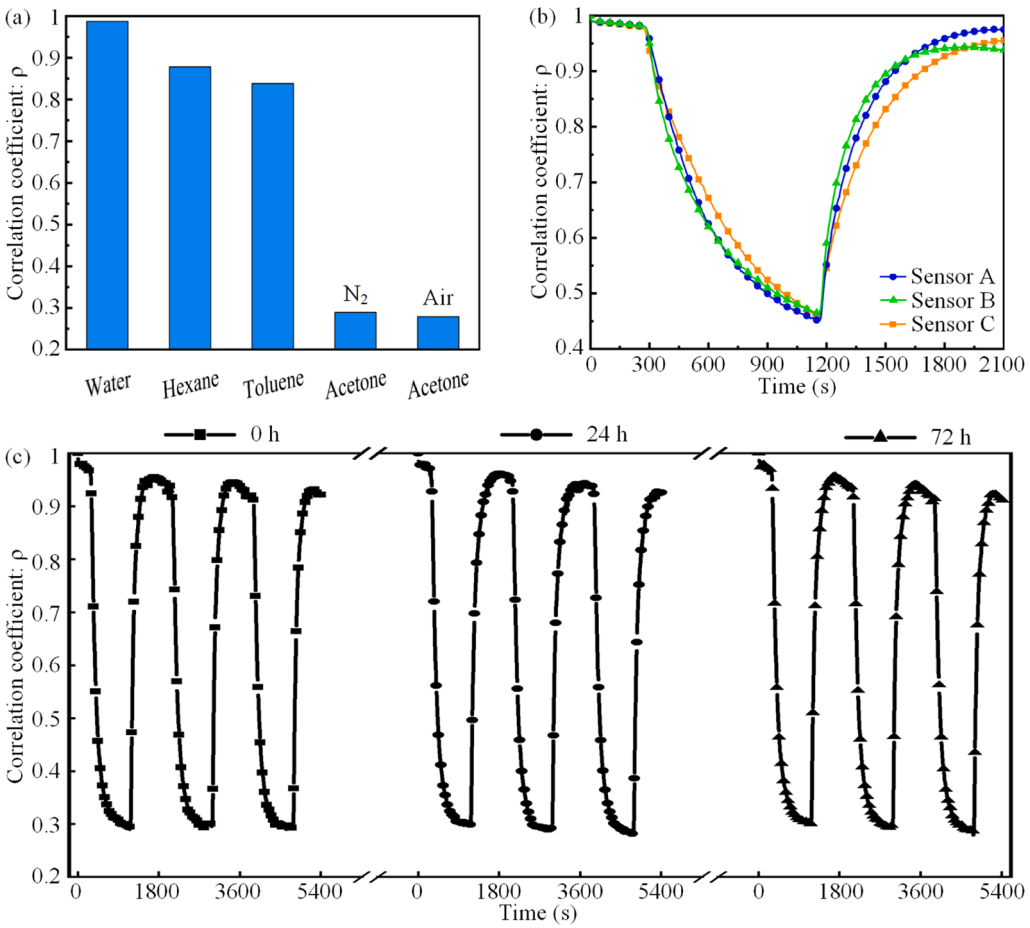

Fig. 5. (a) Response of the LCG film to different vapors at a concentration of 2200 ppm, demonstrating high selectivity toward acetone with nitrogen or air as carrier gas. (b) Consistency test of three LCG films at an acetone vapor concentration of 1400 ppm. (c) Repeatability test and long-term stability test of the LCG film at an acetone vapor concentration of 2200 ppm.

Table 2
The solubility parameters of different chemical substances in the study.

substances	δ_D	δ_P	δ_H	δ
5CB	19.3	8.3	3	21.22
Acetone	15.5	10.4	7	19.94
Toluene	18	1.4	2	18.16
Hexane	14.9	0	0	14.9
Water	15.6	16	42.3	47.84

confined nematic phase temperature range. In future studies, different types of LCs will be employed with the objective of achieving a broader spectrum of operational temperatures; to make the LCG sensor practical, speckle pattern image-processing sub-systems for real-time monitoring and early warning is expected to be developed.

CRediT authorship contribution statement

Suotang Jia: Funding acquisition. **Yifei Ma:** Software, Formal analysis. **Zhaomin Tong:** Writing – review & editing, Validation, Supervision, Project administration, Methodology, Funding acquisition, Conceptualization. **Xuyuan Chen:** Project administration, Funding acquisition. **Yuxiang Yan:** Validation, Investigation. **Ning Bu:** Writing – original draft, Visualization, Software, Methodology, Investigation, Data curation. **Mei Wang:** Validation, Resources. **Xiaoquan Bai:** Data curation.

Declaration of Competing Interest

The authors declare that they have no known competing financial interests or personal relationships that could have appeared to influence the work reported in this paper.

Acknowledgments

This work was supported by the Key Research and Development Program of Shanxi Province (202102030201002); the Changjiang Scholars and Innovative Research Team in University of Ministry of Education of China (IRT_17R70); the State Key Program of National Natural Science of China (11434007); the 111 Project (D18001); the Fund for Shanxi "1331 Project" Key Subjects Construction.

Appendix A. Supporting information

Supplementary data associated with this article can be found in the online version at doi:10.1016/j.snb.2024.136773.

Data availability

Data will be made available on request.

References

[1] X. Mu, H. Ding, W. Pan, Q. Zhou, W. Du, K. Qiu, et al., Research progress in catalytic oxidation of volatile organic compound acetone, J. Environ. Chem. Eng. 9 (2021) 105650, https://doi.org/10.1016/j.jece.2021.105650.

[2] M. Khatib, H. Haick, Sensors for volatile organic compounds, ACS Nano 16 (2022) 7080–7115, https://doi.org/10.1021/acsnano.1c10827.

[3] N. Thongsai, P. Jaiyong, S. Kladsomboon, I. In, P. Paoprasert, Utilization of carbon dots from jackfruit for real-time sensing of acetone vapor and understanding the electronic and interfacial interactions using density functional theory, Appl. Surf. Sci. 487 (2019) 1233–1244, https://doi.org/10.1016/j.apsusc.2019.04.269.

[4] N. Umicevic, J.K. Stevuljevic, V. Paleksic, D.D. Cosic, E.A. Miljakovic, A. B. Djordjevic, Liver function alterations among workers in the shoe industry due to combined low-level exposure to organic solvents, Drug Chem. Toxicol. 45 (2021) 1907–1914, https://doi.org/10.1080/01480545.2021.1894703.

[5] S. Mohammadi, M.H. Zarifi, Differential microwave resonator sensor for real-Time monitoring of volatile organic compounds, IEEE Sens. J. 21 (2021) 6105–6114, https://doi.org/10.1109/JSEN.2020.3041810.

[6] Y. Zhuang, W. Yuan, L. Qian, S. Chen, G. Shi, High-performance gas sensors based on a thiocyanate ion-doped organometal halide perovskite, Phys. Chem. Chem. Phys. 19 (2017) 12876–12881, https://doi.org/10.1039/c7cp01646h.

[7] L. Lyu, Q. Xie, Y. Yang, R. Wang, W. Cen, S. Luo, et al., A novel CeO_2 hollow-shell sensor constructed for high sensitivity of acetone gas detection, Appl. Surf. Sci. 571 (2022) 151337, https://doi.org/10.1016/j.apsusc.2021.151337.

[8] K.G. Krishna, S. Parne, N. Pothukanuri, V. Kathirvelu, S. Gandi, D. Joshi, Nanostructured metal oxide semiconductor-based gas sensors: a comprehensive review, Sens. Actuators, A. 341 (2022) 113578, https://doi.org/10.1016/j.sna.2022.113578.

[9] S. Şen, F.C. Önder, R. Çapan, M. Ay, A room temperature acetone sensor based on synthesized tetranitro-oxacalix [4] arenes: thin film fabrication and sensing properties, Sens Actuators, A 315 (2020) 112308, https://doi.org/10.1016/j.sna.2020.112308.

[10] W. Liu, Z. Liu, Y. Zhang, S. Li, Y. Zhang, X. Yang, et al., Specialty optical fibers and 2D materials for sensitivity enhancement of fiber optic SPR sensors: a review, Opt. Laser Technol. 152 (2022) 108167, https://doi.org/10.1016/j.optlastec.2022.108167.

[11] C. Zhang, A. Ghosh, H. Zhang, S.Q. Shi, Langasite-based surface acoustic wave resonator for acetone vapor sensing, Smart Mater. Struct. 29 (2019) 015039, https://doi.org/10.1088/1361-665X/ab4739.

[12] V.V. Quang, V.N. Hung, V.N. Phan, T.Q. Huy, N.V. Quy, Graphene-coated quartz crystal microbalance for detection of volatile organic compounds at room temperature, Thin Solid Films 568 (2014) 6–12, https://doi.org/10.1016/j.tsf.2014.07.036.

[13] G.T. Fan, C.L. Yang, C.H. Lin, C.C. Chen, C.H. Shih, Applications of Hadamard transform-gas chromatography/mass spectrometry to the detection of acetone in healthy human and diabetes mellitus patient breath, Talanta 120 (2014) 386–390, https://doi.org/10.1016/j.talanta.2013.12.025.

[14] J. King, A. Kupferthaler, B. Frauscher, H. Hackner, K. Unterkofler, G. Teschl, et al., Measurement of endogenous acetone and isoprene in exhaled breath during sleep, Physiol. Meas. 33 (2012) 413, https://doi.org/10.1088/0967-3334/33/3/413.

[15] V.K. Sharma, D. Mohan, P. Sahare, Fluorescence quenching of 3-methyl 7-hydroxyl Coumarin in presence of acetone, Spectrochim. Acta, Part A. 66 (2007) 111–113, https://doi.org/10.1016/j.saa.2006.02.032.

[16] P. Mochalski, J. Rudnicka, A. Agapiou, M. Statheropoulos, A. Amann, B. Buszewski, Near real-time VOCs analysis using an aspiration ion mobility spectrometer, J. Breath. Res. 7 (2013) 026002, https://doi.org/10.1088/1752-7155/7/2/026002.

[17] C. Esteves, E. Ramou, A.R.P. Porteira, A.J.M. Barbosa, A.C.A. Roque, Seeing the unseen: the role of liquid crystals in gas-sensing technologies, Adv. Opt. Mater. 8 (2020) 1902117, https://doi.org/10.1002/adom.201902117.

[18] D.A. Winterbottom, R. Narayanaswamy, Cholesteric liquid crystals for detection of organic vapours, Sens. Actuators, B. 90 (2003) 52–57, https://doi.org/10.1016/S0925-4005(03)00021-2.

[19] K.H. Chan, H.Y. Lin, M.Z. Zhang, Y. Lin, S.J. Hwang, High sensitive cholesteric liquid crystal vapor sensor by using graphene oxide, IEEE Photonics Conf. (IPC) (2016) 777–778, https://doi.org/10.1109/IPCon.2016.7831310.

[20] P. Cachelin, J.P. Green, T. Peijs, M. Heeney, C.W. Bastiaansen, Optical acetone vapor sensors based on chiral nematic liquid crystals and reactive chiral dopants, Adv. Opt. Mater. 4 (2016) 592–596, https://doi.org/10.1002/adom.201500549.

[21] Z. Zhang, A. Bolshakov, J. Han, J. Zhu, K.L. Yang, Electrospun core-sheath fibers with a uniformly aligned polymer network liquid crystal (PNLC), ACS Appl. Mater. Interfaces 15 (2023) 14800–14809, https://doi.org/10.1021/acsami.2c23065.

[22] Z.M. Mykytyuk, I.P. Kremer, M. Ivakh, I.S. Diskovskyi, S.V. Khomyak, Optical sensor with liquid crystal sensitive element for monitoring acetone vapor during exhalation, Mol. Cryst. Liq. Cryst. 721 (2021) 24–29, https://doi.org/10.1080/15421406.2021.1905273.

[23] Z. Liu, D. Luo, K. Yang, Monitoring the two-dimensional concentration profile of toluene vapors by using polymer-stabilized nematic liquid crystals in microchannels, Lab Chip 20 (2020) 1687–1693, https://doi.org/10.1039/C9LC01021A.

[24] D.M.A. Kooijman, C. Robb, Y. Guan, A. Jákli, J.L. West, Liquid crystal core polymer fiber mat electronic gas sensors, Liq. Cryst. 48 (2021) 1880–1887, https://doi.org/10.1080/02678292.2021.1904522.

[25] K.D. Cadwell, M.E. Alf, N.L. Abbott, Infrared spectroscopy of competitive interactions between liquid crystals, metal salts, and dimethyl methylphosphonate at surfaces, J. Phys. Chem. B. 110 (2006) 26081–26088, https://doi.org/10.1021/jp063211k.

[26] D. Cheng, S.S. Sridharamurthy, J.T. Hunter, J.S. Park, N.L. Abbott, H. Jiang, A sensing device using liquid crystal in a micropillar array supporting structure, J. Micro Syst. 18 (2009) 973–982, https://doi.org/10.1109/JMEMS.2009.2029977.

[27] S.K. Pal, A. Agarwal, N.L. Abbott, Chemically responsive gels prepared from microspheres dispersed in liquid crystals, Small 5 (2009) 2589–2596, https://doi.org/10.1002/smll.200900961.

[28] A. Agarwal, E. Huang, S. Palecek, N.L. Abbott, Optically responsive and mechanically tunable colloid-in-liquid crystal gels that support growth of fibroblasts, Adv. Mater. 20 (2008) 4804–4809, https://doi.org/10.1002/adma.200800932.

[29] S. Kulkarni, S. Kumar, P. Thareja, Colloidal and fumed particles in nematic liquid crystals: self-assembly, confinement and implications on rheology, J. Mol. Liq. 336 (2021) 116241, https://doi.org/10.1016/j.molliq.2021.116241.

[30] A. Agarwal, S. Sidiq, S. Setia, E. Bukusoglu, J.J. de Pablo, S.K. Pal, et al., Colloid-in-liquid crystal gels that respond to biomolecular interactions, Small 9 (2013) 2785–2792, https://doi.org/10.1002/smll.201202869.

[31] S. Han, K. Lee, S.E. Shim, P.J. Saikia, S. Choe, I. Cheong, Electrolyte effect on the particle characteristics prepared by soap-free emulsion polymerization, Macromol. Res. 15 (2007) 403–411, https://doi.org/10.1007/BF03218806.

[32] J. Hong, H. Han, C.K. Hong, S.E. Shim, A direct preparation of silica shell on polystyrene microspheres prepared by dispersion polymerization with polyvinylpyrrolidone, J. Polym. Sci., Part A: Polym. Chem. 46 (2008) 2884–2890, https://doi.org/10.1002/pola.22624.

[33] Y. Bai, X. Luo, Y. Han, B. Liu, J. Zhang, M. Zhang, Facile synthesis of narrow particle size distribution, high solid content, cationic polymer latexes by macroemulsion polymerization-based particle coagulation mechanism, J. Macromol. Sci., Part A: Pure Appl. Chem. 57 (2020) 116–122, https://doi.org/10.1080/10601325.2019.1673175.

[34] S. Yun, J. Kim, Multi-walled carbon nanotubes–cellulose paper for a chemical vapor sensor, Sens. Actuators, B. 150 (2010) 308–313, https://doi.org/10.1016/j.snb.2010.06.068.

[35] R. Blue, Z. Vobecka, P.J. Skabara, D. Uttamchandani, The development of sensors for volatile nitro-containing compounds as models for explosives detection, Sens. Actuators, B. 176 (2013) 534–542, https://doi.org/10.1016/j.snb.2012.10.088.

[36] J.A. Dean. Lange's Handbook of Chemistry, fifteenth ed., McGraw-Hill, 1999.

[37] F. Mondiot, X. Wang, J.J. de Pablo, N.L. Abbott, Liquid crystal-based emulsions for synthesis of spherical and non-spherical particles with chemical patches, J. Am. Chem. Soc. 135 (2013) 9972–9975, https://doi.org/10.1021/ja4022182.

[38] I. Kim, W.S. Kim, K. Kim, M.A. Ansari, M.Q. Mehmood, T. Badloe, et al., Holographic metasurface gas sensors for instantaneous visual alarms, Sci. Adv. 7 (2021) eabe9943, https://doi.org/10.1126/sciadv.abe9943.

[39] J.W. Goodman, Speckle Phenomena in Optics: Theory and Applications, Roberts and Company Publishers, Greenwood Village, CO 80111, USA, 2007.

[40] Z. Tong, X. Chen, Speckle contrast for superposed speckle patterns created by rotating the orientation of laser polarization, J. Opt. Soc. Am. A. 29 (2012) 2074–2079, https://doi.org/10.1364/JOSAA.29.002074.

[41] Y.J. Liu, X.W. Sun, Holographic polymer-dispersed liquid crystals: Materials, formation, and applications, Adv. OptoElectron. 2008 (2008) 684349, https://doi.org/10.1155/2008/684349.

[42] H. Ono, H. Shimokawa, A. Emoto, N. Kawatsuki, Effects of droplet size on photorefractive properties of polymer dispersed liquid crystals, Polymer 44 (2003) 7971–7978, https://doi.org/10.1016/j.polymer.2003.10.038.

[43] E. Bukusoglu, S.K. Pal, J.J. de Pablo, N.L. Abbott, Colloid-in-liquid crystal gels formed via spinodal decomposition, Soft Matter 10 (2014) 1602–1610, https://doi.org/10.1039/C3SM51877A.

[44] K. Schelski, C.G. Reyes, L. Pschyklenk, P.M. Kaul, J.P.F. Lagerwall, Quantitative volatile organic compound sensing with liquid crystal core fibers, Cell Rep. Phys. Sci. 2 (2021) 100661, https://doi.org/10.1016/j.xcrp.2021.100661.

[45] J.K. Gupta, J.S. Zimmerman, J.J. de Pablo, F. Caruso, N.L. Abbott, Characterization of adsorbate-induced ordering transitions of liquid crystals within monodisperse droplets, Langmuir 25 (2009) 9016–9024, https://doi.org/10.1021/la900786b.

[46] T. Yamamoto, M. Yoshida, Viscoelastic and photoresponsive properties of microparticle/liquid-crystal composite gels: tunable mechanical strength along with rapid-recovery nature and photochemical surface healing using an azobenzene dopant, Langmuir 28 (2012) 8463–8469, https://doi.org/10.1021/la3001784.

[47] N. Mac, Fhionnlaoich, S. Schrettl, N.B. Tito, Y. Yang, M. Nair, L.A. serrano, et al., Reversible microscale assembly of nanoparticles driven by the phase transition of a thermotropic liquid crystal, ACS Nano 17 (2023) 9906–9918, https://doi.org/10.1021/acsnano.2c09203.

[48] P.G. Petrov, E.M. Terentjev, Formation of cellular solid in liquid crystal colloids, Langmuir 17 (2001) 2942–2949, https://doi.org/10.1021/la0016470.

[49] E. Bukusoglu, M.B. Pantoja, P.C. Mushenheim, X. Wang, N.L. Abbott, Design of responsive and active (soft) materials using liquid crystals, Annu. Rev. Chem. Biomol. Eng. 7 (2016) 163–196, https://doi.org/10.1146/annurev-chembioeng-061114-123323.

[50] F. Xu, C. Zhou, A rule for operation temperature selection of a conductometric VOC gas sensor based on ZnO nanotetrapods, J. Alloy. Compd. 858 (2021) 158294, https://doi.org/10.1016/j.jallcom.2020.158294.

[51] R. Capan, I. Capan, M. Bayrakci, Rhodamine-based electrospun polyacrylonitrile (PAN) nanofiber sensor for the detection of chlorinated hydrocarbon vapors, ACS Appl. Polym. Mater. 6 (2024) 7500–7511. ⟨https://doi-org.chula.pub-online.com/10.1021/acsapm.4c00909⟩.

[52] L.W. Honaker, S. Vats, M. Anyfantakis, J.P.F. Lagerwall, Elastic sheath–liquid crystal core fibres achieved by microfluidic wet spinning, J. Mater. Chem. C 7 (2019) 11588, https://doi.org/10.1039/C9TC03836A.
[53] L.R. Mikael, Hansen solubility parameters and SWCNT composites. In: Procedings of the 17th International Conference on Composite Materials (ICCM-17). (2009).
[54] S. Gårdebjer, M. Andersson, J. Engström, P. Restorp, M. Persson, A. Larsson, Using Hansen solubility parameters to predict the dispersion of nano-particles in polymeric films, Polym. Chem. 7 (2016) 1756, https://doi.org/10.1039/C5PY01935D.

Ning Bu received the B.E. degree from the Inner Mongolia University of Science and Technology, China, in 2021. He is currently pursuing the M.S. degree in Electronic Information in the Institute of Laser Spectroscopy of Shanxi university, China. His current research interest includes gas sensing based on laser speckle.

Yuxiang Yan received the B.E. degree from the Tianjin University of Technology and Education, China, in 2020. He is currently pursuing the Ph.D. degree in Atomic and Molecular Physics in the Institute of Laser Spectroscopy of Shanxi university, China. His current research interest includes gas sensing based on laser speckle.

Xiaoquan Bai received the B.E. degree from the Taiyuan University of Science and Technology, China, in 2021. He is currently pursuing the M.S. degree in Optical Engineering in the Institute of Laser Spectroscopy of Shanxi university, China. His current research interest includes gas sensing based on laser speckle.

Mei Wang received the Ph.D. degree from the Sungkyunkwan University, South Korea, in 2014. She worked as a Postdoctoral Researcher with Sungkyunkwan University, until 2017. She is currently a Professor with the State Key Laboratory of Quantum Optics and Quantum Optics Devices, Institute of Laser Spectroscopy, Shanxi University, China. Her research interests include graphenebased materials, electrophoretic deposition, electrode materials for energy storage devices, and electrochemical sensing.

Yifei Ma received the Ph.D. degree from the Sungkyunkwan University, South Korea, in 2016. He is currently an Associate Professor with the State Key Laboratory of Quantum Optics and Quantum Optics Devices, Institute of Laser Spectroscopy, Shanxi University, China. His research interest includes synthesis and functionalization of low-dimensional materials and the applications.

Suotang Jia received the Ph.D. degree from East China Normal University, China, in 1994. From 1997–2000, he was the Director of the Department of Electronics and Information Technology, Shanxi University, China. From 2000–2010, he was the Vice President of the Shanxi University, and the Director of the Optics Institute of Shanxi. From 2010–2012, he was the President of the North University of China. From 2012–2018, he was the President of Shanxi University. His research interest includes laser spectroscopy and quantum optics.

Xuyuan Chen is a distinguished professor at Shanxi University and a permanent professor at the University College of Southeast Norway. His main research fields include laser display, micro-energy, terahertz.

Zhaomin Tong received the Ph.D. degree in electronics and telecommunication from the Norwegian University of Science and Technology, Norway, in 2013. He is currently an Associate Professor with the State Key Laboratory of Quantum Optics and Quantum Optics Devices, Institute of Laser Spectroscopy, Shanxi University, China. His research interests include laser applications and micro-nano technology.